

The primary and secondary electrocaloric effect at ferroelectric-ferroelectric transitions in lead-free ceramics

Haoyu Wang^{a,1}, Le Zhang^{a,1,*}, Yunlong Sun^a, Claudio Cazorla^a, Mengyao Guo^b, Ying Li^c, Kwok Ho Lam^c, Xiaojie Lou^b, Danyang Wang^{a,*}

^a School of Materials Science and Engineering, UNSW, Sydney, NSW 2052, Australia

^b Frontier Institute of Science and Technology and State Key Laboratory for Mechanical Behavior of Materials, Xi'an Jiaotong University, Xi'an 710049, China

^c Department of Electrical Engineering, The Hong Kong Polytechnic University, Hung Hom, Kowloon, Hong Kong, China

ARTICLE INFO

Article history:

Received 17 September 2019

Revised 23 October 2019

Accepted 7 November 2019

Keywords:

Primary electrocaloric effect
Secondary electrocaloric effect
Phonon vibrational entropy

ABSTRACT

Secondary electrocaloric effect (ECE) arising from piezoelectricity combined with crystal thermal expansion was often overlooked in ECE studies of ferroelectric ceramics. This work mainly evaluated the primary ECE (ΔT_{ECE}) and secondary ECE (ΔT_2) of eco-friendly $\text{BaSn}_x\text{Ti}_{1-x}\text{O}_3$ ($\text{BSnT}100x$, $0 < x < 12\%$) ceramics near the tetragonal (T)-orthorhombic (O) transition. Intriguingly, a maximum overall $\Delta T \sim 0.85$ K was obtained at the T-O transition (~ 300 K) of $\text{BSnT}2$ under an electric field of 2 kV/mm, with ΔT_{ECE} and ΔT_2 amounting to ~ 0.75 K, ~ 0.1 K, respectively. This ECE result is $\sim 40\%$ superior than the larger ECE reported previously for BSnT system.

© 2019 Acta Materialia Inc. Published by Elsevier Ltd. All rights reserved.

Electrocaloric effects (ECE) in polar materials result from entropy variations induced by external electric fields, E , which are typically associated with changes in the polarization [1,2]. In the context of developing new eco-friendly cooling technology as an alternative to traditional vapor-compression refrigeration, ECE has emerged as a promising enabler owing to the high cooling efficiency and cost-effectiveness [1,3–5]. Previous studies have revealed that ECE in polar materials depend critically on the phase-transition type (i.e., ferroelectric-paraelectric or ferroelectric-ferroelectric) [6–9], and usually exhibit maximum amplitude at temperatures close to the Curie point (T_c , associated with ferroelectric-paraelectric phase transition) [8]. For instance, in 2006 a huge adiabatic temperature change (ΔT) of ~ 12 K was found in $\text{Pb}(\text{Zr}_{0.95}\text{Ti}_{0.05})\text{O}_3$ thin films at $T_c \sim 222$ °C and $E = 48$ kV/mm [2]. Since then, several lead-based ferroelectric thin films presenting large ΔT have been discovered [4,10,11]. Nevertheless, thin films have much smaller thermal mass than their bulk counterparts which limits their use in large-scale refrigeration applications [12]. In this sense, lead-based ferroelectric ceramics can be regarded as promising inorganic ECE materials.

However, the major concern on the aforementioned lead-based ECE materials lies in their toxicity due to lead content. To address this issue, ECE in lead-free inorganic BaTiO_3 (BTO) ferroelectrics have been investigated. In BTO single crystals, the maximum ΔT occurs at $T_c = 129$ °C and amounts to 0.9 K under an electric field of 1.2 kV/mm [5]. In BTO ceramics, the ΔT ascribed to the same ferroelectric-paraelectric phase transition turns out to be 0.4 K and occurs around $T_c = 118$ °C and $E = 0.75$ kV/mm [13]. In order to bring T_c closer to room temperature, chemical doping strategies have been explored. Interestingly, in Sn-doped BTO (BSnT) ceramics T_c can be shifted down to around 300 K [14–16], and the maximum ΔT measured in that case is 0.61 K under $E = 2$ kV/mm [14,17]. In addition, the ferroelectric-ferroelectric (tetragonal (T)-orthorhombic (O)) phase transition occurring in the same material may also render large ECE as well, due to the possible large entropy change associated with the rotation between the differently oriented polarizations driven by E . [6,9] However, the ECE at ferroelectric-ferroelectric transitions have not attracted much attention due to its present inferior cooling performance to that of T_c [17,18].

Meanwhile, all ferroelectric materials are expected to exhibit secondary electrocaloric effect due to the existence of thermal expansion and piezoelectric effect [19,20]. Such secondary effect can be intuitively understood by the vibrational entropy changes induced by thermal expansion combined with piezoelectricity [20]. As a consequence, the total adiabatic temperature change in ferroelectric polar materials, ΔT , should contain a primary

* Corresponding authors.

E-mail addresses: le.zhang1@unsw.edu.au (L. Zhang), dy.wang@unsw.edu.au (D. Wang).

¹ Mr. Haoyu Wang and Dr. Le Zhang contributed equally to this work (co-first author).

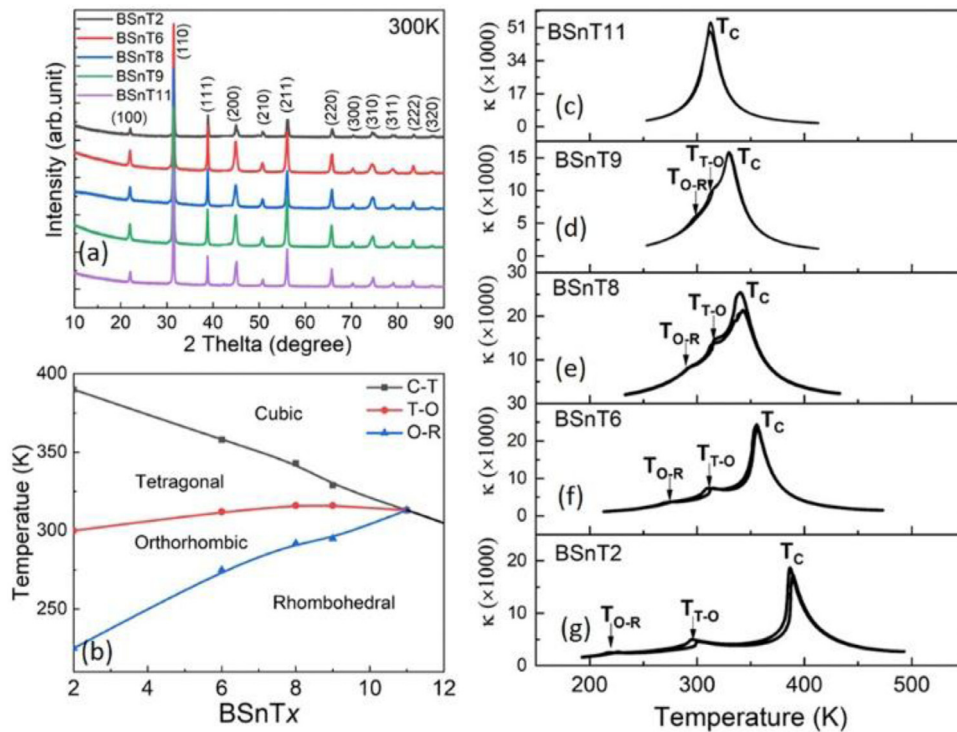


Fig. 1. (a) X-ray diffraction patterns of the $\text{BaSn}_x\text{Ti}_{1-x}\text{O}_3$ ceramics ($x=2\%$, 6%, 8%, 9% and 11%) at 300 K (b) Phase diagram of the $\text{BaSn}_x\text{Ti}_{1-x}\text{O}_3$ ceramics ($0 < x < 12\%$). (c)–(g) show the temperature-dependent dielectric constant (κ) curves of BSNT11, BSNT9, BSNT8, BSNT6 and BSNT2 ceramics at the frequency of 1 kHz, respectively.

ECE (ΔT_{ECE}) and a secondary ECE (ΔT_2) contribution, namely, $\Delta T = \Delta T_{\text{ECE}} + \Delta T_2$. The experiments based on direct or quasi-direct ECE measurements, obtain ΔT directly [21,22]. However, indirect ECE measurements (the vast majority of reported studies) normally work out ΔT_{ECE} only. Consequently, the secondary electrocaloric effect has rarely been reported in previous ECE studies. To the best of our knowledge, only the secondary ECE for $\text{PbZr}_{1-x}\text{Ti}_x\text{O}_3$ thin films or some polymers were reported, rather than any lead-free ceramics [20,23–25].

In this work, we estimated the contributions of primary and secondary electrocaloric effect through analysing the pyroelectric coefficient ($\partial P/\partial T$) components at ferroelectric-ferroelectric transitions in $\text{BaSn}_x\text{Ti}_{1-x}\text{O}_3$ (BSNT100x, $0 < x < 12\%$) ceramics. BSNT ceramics can be regarded as a model system in which secondary electrocaloric effect is expected to be large because of sizeable piezoelectric coefficients and possible thermal strain change near its first-order ferroelectric-ferroelectric (T-O) transitions [15,26]. Our results show that the sign and strength of secondary effect at T-O transitions of BSNT ceramics can affect the cooling performance in a significant manner and are highly dependent on the composition. Especially, a large ΔT of ~ 0.85 K (wherein $\Delta T_{\text{ECE}} \sim 0.75$ K and $\Delta T_2 \sim 0.1$ K) is discovered at the T-O transition (~ 300 K) of BSNT2 under an electric field of 2 kV/mm, which is much higher than the best reported $\Delta T_{\text{ECE}} \sim 0.61$ K (under 2 kV/mm) at tricritical point in BSNT ceramics [14,17]. In view of our results, previous ECE reports based on the indirect method and that were performed in the vicinity of phase transitions displaying high piezoelectricity, may need some revisions.

$\text{BaSn}_x\text{Ti}_{1-x}\text{O}_3$ ($x=2\%$, 6%, 8%, 9%, 11%, abbreviated as BSNT2, BSNT6, BSNT8, BSNT9 and BSNT11, respectively) ceramics were synthesized using conventional solid-state sintering process with the starting chemicals of BaCO_3 (Alfa Aesar, 99.9%), TiO_2 (Alfa Aesar, 99.9%) and SnO_2 (Alfa Aesar, 99.9%). The sintering was conducted at 1400 °C–1450 °C for 3–4 h. The temperature dependence of polarization–electric field (P–E) hysteresis loops were measured by a TF Analyser 2000 ferroelectric workstation con-

nected with a temperature-controlled chamber. The thermal expansion (ϵ – T) curves were obtained by a thermal mechanical analyser (TMA-8310, Rigaku) under a constant test stress of 0.03 N. The crystal structure was characterized by X-ray diffractometer (XRD, MPD PANalytical). The temperature-dependent dielectric permittivity curves were obtained using an LCR meter (Agilent, E4980 Precision LCR Meter) with a temperature-controlled sample stage (Linkam HFS600E-PB4).

Fig. 1(a) shows the XRD diffraction patterns of $\text{BaSn}_x\text{Ti}_{1-x}\text{O}_3$ ceramics at 300 K in the 2θ range of 10° – 90° , confirming the pure perovskite structure of the ceramics without any impurities or secondary phases. Fig. 1(c)–(g) shows the dielectric constant vs. temperature curves of BSNT11, BSNT9, BSNT8, BSNT6 and BSNT2 ceramics, respectively, during heating and cooling. The peaks and bulges in the temperature-dependent dielectric curves suggest the phase transitions, including cubic (C)–tetragonal (T) (T_c), tetragonal (T)–orthorhombic (O) (T_{T-O}) and orthorhombic (O)–rhombohedral (R) (T_{O-R}). The $\text{BaSn}_x\text{Ti}_{1-x}\text{O}_3$ ($0 < x < 12\%$) phase diagram shown in Fig. 1(b) is constructed based on the temperature-dependent dielectric data gathered during heating (see Fig. 1(c)–(g)). It is clearly shown that T_c decreases while both T_{T-O} and T_{O-R} increase upon increase in Sn doping level, which is in good agreement with previous studies [14,15]. The low thermal hysteresis of the rounded dielectric peak at T_{T-O} at $6 \leq x \leq 9\%$ indicates the first-order transition is weakened with doping more Sn, in contrast to the strong first-order T-O transition (~ 300 K) observed in BSNT2 ($x=2\%$) ceramics (which displays higher dielectric thermal hysteresis with sharp dielectric peaks) [27,28]. The strong first-order transition in ferroelectrics always accompanies large polarization change and coupled thermal strain variations. Further, the T, O and R phases are merged into a phase coexistence region with the C phase near $x=11\%$ [14,15]. A sharp enhancement in piezoelectric response has been observed at the T-O transition in BSNT ($0 < x < 12\%$) ceramics near room temperature and explained by the lower polarization anisotropy induced by the tricritical point existing near phase coexistence region [28–30]. Therefore, it is expected that consider-

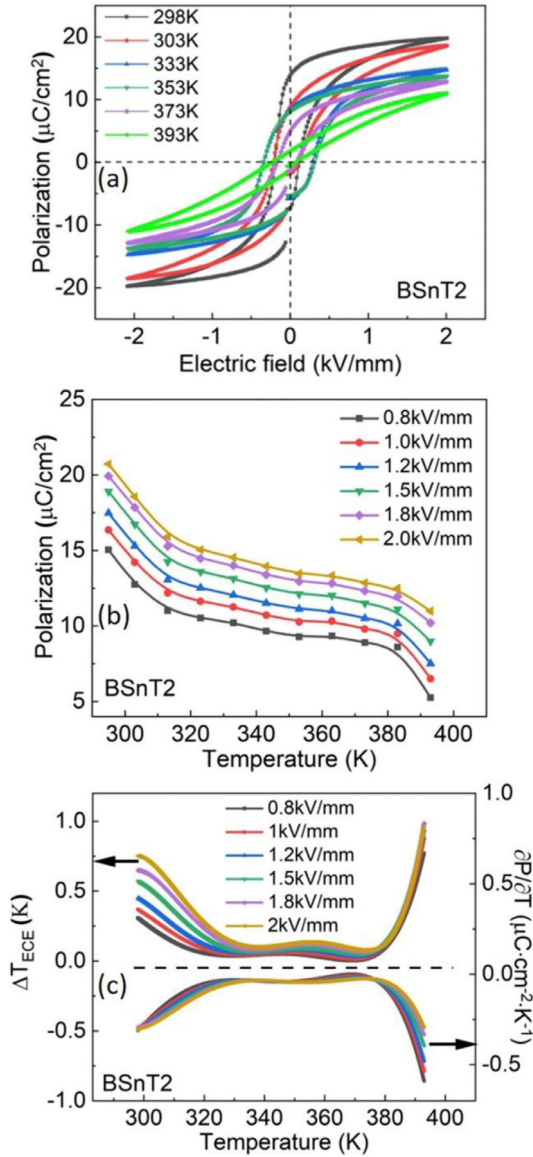


Fig. 2. (a) P–E hysteresis loops of BSnT2 ceramics under 2 kV/mm at different temperatures upon heating; Temperature dependence of (b) P_m , (c) ΔT_{ECE} (left y axis) and $\partial P/\partial T$ (right y axis) of BSnT2 ceramics under different electric fields. P_m was extracted from the P–E loops upon heating.

able secondary electrocaloric effects as well as large primary ECE will be appreciable at the T-O transitions of BSnT2 due to the strong first-order transition features and high piezoelectricity.

Fig. 2(a) displays the temperature-dependent P–E loops in BSnT2 ceramics, measured at a frequency of 1 Hz and under an electric field of 2 kV/mm during heating. The saturation polarization (P_m) in BSnT2 samples decreases gradually as the temperature increases, due to the thermal evolution of ferroelectric domains while approaching T_c [31]. The temperature-dependent P–E loops corresponding to other compositions, shown in Figs. S1 (see supplementary materials), are also well-saturated under 2 kV/mm.

Fig. 2(b) shows the evolution of P_m as a function of temperature in BSnT2 ceramics for different electric fields. Besides the general polarization reduction trend under increasing temperature, the P_m –T curves exhibit two clear slope-changing points at around 300 K and 380 K, which correspond to T_{T-O} and T_c , respectively. To calculate the adiabatic temperature change associated to the primary electrocaloric effect, ΔT_{ECE} , we employ the usual formula

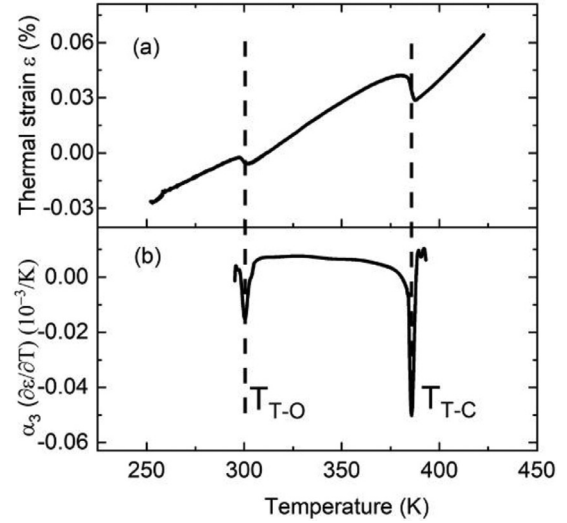


Fig. 3. Temperature dependence of (a) thermal strain ε and (b) thermal expansion coefficient α_3 of BSnT2 ceramics upon heating.

[32,33]:

$$\Delta T_{ECE} = -\frac{T}{\rho C_p} \int_0^E \left(\frac{\partial P}{\partial T} \right) dE \quad (1)$$

where ρ represents the density and C_p the heat capacity at ambient pressure. Here, temperature dependent C_p is obtained, which is the same level as reported $\sim 0.4 \text{ J}/(\text{gK})$ [12]. The density values of the samples, as determined by the Archimedes' method, amount to $5.8\text{--}6.1 \text{ g}/\text{cm}^3$. The $(\partial P/\partial T)_{ECE}$ values entering Eq. (1) (see bottom of Fig. 2(c)) were obtained with a six-order polynomial fit to the measured P_m –T curves enclosed in Fig. 2(b). The ΔT_{ECE} calculated in BSnT2 as a function of temperature and electric field are displayed in top of Fig. 2(c). Two maximum ΔT_{ECE} values appear at around 300 K ($\Delta T_{ECE} \sim 0.75 \text{ K}$) and 380 K ($\Delta T_{ECE} \sim 1.0 \text{ K}$) which are attributed to the T-O and T-C phase transitions respectively and much higher than the values reported by Upadhyay et al. [18], Zhang et al. [34] and Luo et al. [14]. Both ΔT_{ECE} peaks have positive values due to the fact that the crystal experiences an entropy decrease when E-driven polarization ordering is built in ferroelectrics (we recall that in caloric materials isothermal entropy and adiabatic temperature increments always present opposite signs, namely, $\Delta S < 0$ implies $\Delta T > 0$ and *vice versa*).

The contribution of secondary electrocaloric component ΔT_2 at phase transitions along the poling direction can be estimated using the formula [20]:

$$\Delta T_2 = -\frac{T}{\rho C_p} \int_0^E \alpha_3 d_{33} c_{33} dE \quad (2)$$

where d_{33} is the direct piezoelectric coefficient along the poling direction (extracted from Yao's et al. work [15]), α_3 the thermal expansion coefficient and c_{33} the elastic constant ($\sim 80 \text{ GPa}$ [35]). In practice, we considered that the dependence of α_3 on E is weak within the interval $0 \leq E \leq 2 \text{ kV/mm}$.

Fig. 3(a) shows the temperature dependence of thermal strain ε ($\Delta L/L$) of BSnT2 ceramics. T-O and C-T phase transitions are indicated as the two sharp ε drops near 300 K and 380 K, respectively [14,15]. The temperature dependence of thermal expansion coefficient α_3 ($\partial \varepsilon/\partial T$) value is depicted in Fig. 3(b). The ΔT_2 at the T-O transition of BSnT2 ($d_{33} = 300 \text{ pC/N}$ obtained under a constant stress of 0.25 N [15]) was calculated to be 0.1 K , which is 13.3% of that of primary effect ΔT_{ECE} , namely 0.75 K , suggesting a positive effect to the overall cooling capability. Thus, the ΔT at the T-O transition of BSnT2 is $\sim 0.85 \text{ K}$ ($\Delta T = \Delta T_{ECE} + \Delta T_2 = 1.133 * \Delta T_{ECE}$)

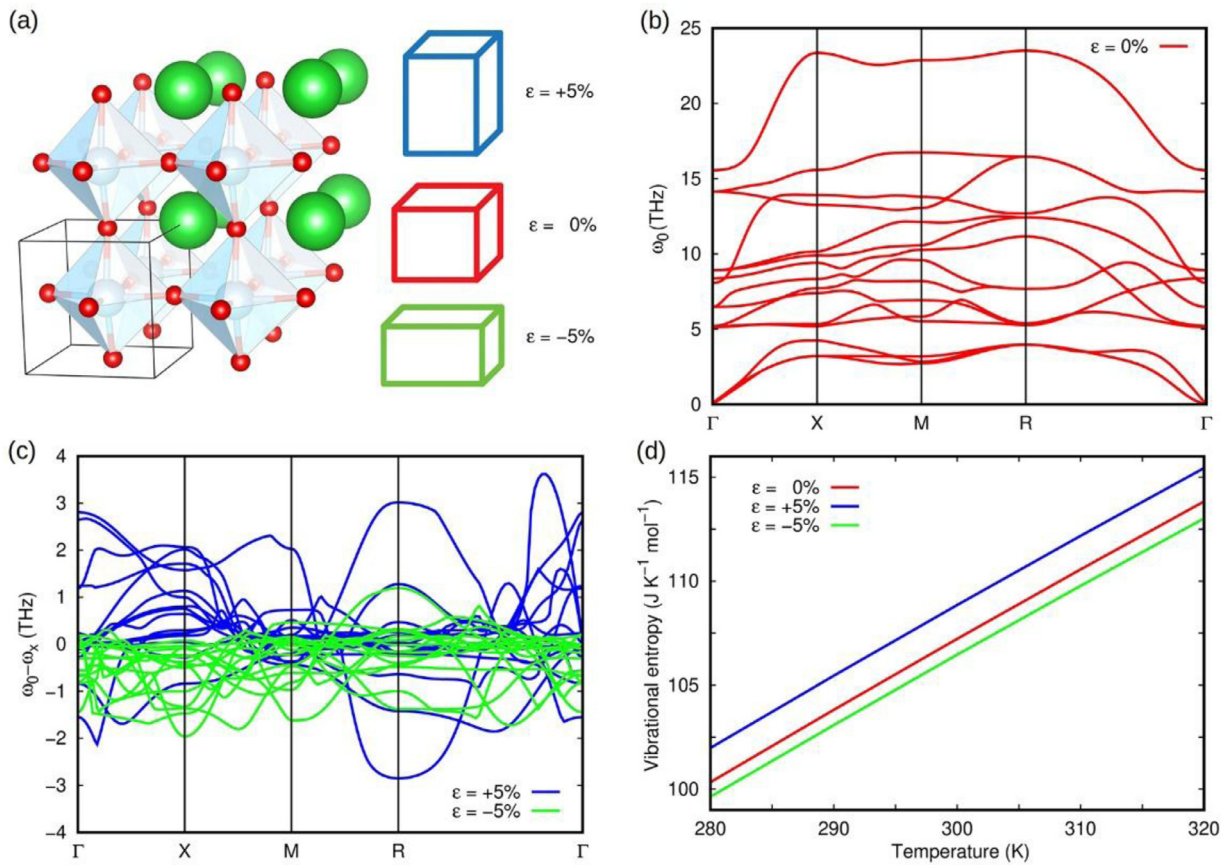


Fig. 4. First-principles calculations based on density functional theory performed in strained and unstrained BaTiO₃. (a) Sketch of the unit cells considered in the simulations. (b) Phonon spectrum calculated at null uniaxial strain. (c) Vibrational phonon frequency differences calculated between the +5% strained and -5% strained crystals. (d) Vibrational entropy estimated in +5%, -5% strained and unstrained BaTiO₃ as a function of temperature.

Table 1
Piezoelectric coefficient d_{33} , and primary, secondary and total ECE strengths at T-O transitions of BSNT ceramics.

Sample	d_{33} (pC/N) [15]	ΔT_{ECE} (K)	ΔT_2 (K)	$\Delta T_2/\Delta T_{\text{ECE}}$	$\Delta T = \Delta T_{\text{ECE}} + \Delta T_2$
BSnT2	300	0.75 K	0.10 K	+13.3%	0.85 K
BSnT6	500	0.25 K	0.006 K	+2.4%	0.256 K
BSnT8	550	0.27 K	-0.054 K	-20%	0.216 K
BSnT9	600	0.27 K	-0.027 K	-10%	0.243 K
BSnT11	700	0.6 K	-0.09 K	-15%	0.51 K

under 2 kV/mm. This value is much higher than the best-reported $\Delta T_{\text{ECE}} \sim 0.61$ K in BSNT ceramics, which will be potential for cooling applications [14,17].

It is known that positive thermal expansion coefficient outside the phase transition region in Fig. 3(b) will render negative sign for ΔT_2 [20]. Why can ΔT_2 present a positive sign at T-O transitions of BSnT2 and result in larger ΔT ? Typically, most vibrational phonon frequencies in polar crystals decrease under increasing temperature due to lattice expansion [20]. Such a lattice vibration softening produces an increase in the vibrational entropy of the crystal ($\Delta S_{\text{vib}} > 0$), hence the secondary electrocaloric effect turns out to be negative as usual and adverse to the primary ECE. But the lattice parameter difference in the O and T phases here renders a contraction in volume (see Fig. 3(a)), resulting in a steep drop in thermal strain ϵ during the T-O transition upon heating. Thus, a positive secondary ECE is observed as due to hardening of the phonon frequencies and decrease in vibrational entropy ($\Delta S_{\text{vib}} < 0$). In order to explicitly demonstrate this effect above, we have conducted first-principles calculations based on density functional theory (DFT) to estimate the vibrational entropy of bulk BaTiO₃ (BTO) with by considering different uniaxial strain condi-

tions (namely, equilibrium, +5%, and -5% strain along the c lattice vector direction). The details of DFT calculation method is shown in supporting materials. Fig. 4 encloses the results of our DFT simulations, which clearly show that the vibrational entropy in the uniaxially stretched crystal is larger than that in the $\epsilon = 0$ due to lattice softening (Fig. 4(b) and (c)), whereas the $\epsilon = -5\%$ (uniaxially compressed) cases exhibit lower vibrational entropy compared with the unstrained state.

Furthermore, we also studied the temperature dependence of ΔT_{ECE} and $\partial P/\partial T$, ϵ and α_3 ($\partial \epsilon/\partial T$) for compositions other than BSnT2, which are shown in Figs. S2 and S3 (see supplementary materials). It is noted that the absolute values of ΔT_{ECE} significantly decrease when Sn doping increases from 2% to 9%. This effect is presumably ascribed to the lowering of T_c and polarization anisotropy at higher Sn concentration [14,15]. The ΔT_{ECE} enhancement at the phase convergence region ($x = 11\%$, Fig. S2(d)) can be attributed to the large entropy change caused by E-induced phase transitions among the four possible states. The strength of the primary and secondary ECE at the T-O transition of BSNT ceramics are summarized in Table 1. Intriguingly, the secondary effect contributes positively to the total ECE for $x \leq 6\%$, whereas negatively

for $x > 7\%$. The ΔT_2 behavior depends on the sign of the thermal expansion coefficient α_3 at the T-O phase transitions upon heating. With increasing Sn content up to $x > 7\%$, which is near to the phase convergence region at $x = 11\%$ with tricritical phase transition behavior [14,15], the T-O transition exhibits decreased polarization anisotropy which results in a lower crystal volume change and positive sign of α_3 (corresponding to negative ΔT_2) at the T-O transition upon heating. Consequently, the sign and strength of the secondary effect at the T-O transition are highly dependent on composition and can affect the total ECE significantly, i.e., +13.3% at T-O transition for BSNT2 and up to -20% for BSNT8. It can be further concluded that the contribution of secondary electrocaloric effect at ferroelectric-ferroelectric phase transitions must be taken into account when estimating cooling capability of bulk ferroelectrics using indirect method.

Financial supports from the Australian Research Council (DP170103514, FT180100541, and FT140100135) and National Natural Science Foundation of China (Grant no. 51772238) are acknowledged.

Declaration of Competing Interest

We declare that there are no interests conflict in this work.

Supplementary material

Supplementary material associated with this article can be found, in the online version, at doi:10.1016/j.scriptamat.2019.11.014.

References

- [1] B. Neese, B. Chu, S.-G. Lu, Y. Wang, E. Furman, Q.M. Zhang, *Science* 321 (5890) (2008) 821.
- [2] A.S. Mischenko, Q. Zhang, J.F. Scott, R.W. Whatmore, N.D. Mathur, *Science* 311 (5765) (2006) 1270.
- [3] R. Ma, Z. Zhang, K. Tong, D. Huber, R. Kornbluh, Y.S. Ju, Q. Pei, *Science* 357 (6356) (2017) 1130.
- [4] B. Peng, H. Fan, Q. Zhang, *Adv. Funct. Mater.* 23 (23) (2013) 2987–2992.
- [5] X. Moya, E. Stern-Taulats, S. Crossley, D. González-Alonso, S. Kar-Narayan, A. Planes, L. Mañosa, N.D. Mathur, *Adv. Mater.* 25 (9) (2013) 1360–1365.
- [6] Y. Zhou, Q. Lin, W. Liu, D. Wang, *RSC Adv.* 6 (17) (2016) 14084–14089.
- [7] Y. Bai, X. Han, L. Qiao, *Appl. Phys. Lett.* 102 (25) (2013) 252904.
- [8] M. Valant, *Prog. Mater. Sci.* 57 (6) (2012) 980–1009.
- [9] M. Marathe, D. Renggli, M. Sanlialp, M.O. Karabasov, V.V. Shvartsman, D.C. Lupascu, A. Grünebohm, C. Ederer, *Phys. Rev. B* 96 (1) (2017) 014102.
- [10] S.G. Lu, B. Rožič, Q.M. Zhang, Z. Kutnjak, X. Li, E. Furman, L.J. Gornoy, M. Lin, B. Malič, M. Kosec, R. Blinc, R. Pirc, *Appl. Phys. Lett.* 97 (16) (2010) 162904.
- [11] T.M. Correia, J.S. Young, R.W. Whatmore, J.F. Scott, N.D. Mathur, Q. Zhang, *Appl. Phys. Lett.* 95 (18) (2009) 182904.
- [12] M.-D. Li, X.-G. Tang, S.-M. Zeng, Q.-X. Liu, Y.-P. Jiang, T.-F. Zhang, W.-H. Li, *ACS Sustain. Chem. Eng.* 6 (7) (2018) 8920–8925.
- [13] A. Karchevskii, *Sov. Phys. Solid State* 3 (10) (1962) 2249–2254.
- [14] Z. Luo, D. Zhang, Y. Liu, D. Zhou, Y. Yao, C. Liu, B. Dkhil, X. Ren, X. Lou, *Appl. Phys. Lett.* 105 (10) (2014) 102904.
- [15] Y. Yao, C. Zhou, D. Lv, D. Wang, H. Wu, Y. Yang, X. Ren, *EPL Europhys. Lett.* 98 (2) (2012) 27008.
- [16] C. Lei, A.A. Bokov, Z.G. Ye, *J. Appl. Phys.* 101 (8) (2007) 084105.
- [17] M. Sanlialp, Z. Luo, V.V. Shvartsman, X. Wei, Y. Liu, B. Dkhil, D.C. Lupascu, *Appl. Phys. Lett.* 111 (17) (2017) 173903.
- [18] S.K. Upadhyay, V.R. Reddy, P. Bag, R. Rawat, S.M. Gupta, A. Gupta, *Appl. Phys. Lett.* 105 (11) (2014) 112907.
- [19] Y. Liu, I.C. Infante, X. Lou, L. Bellaiche, J.F. Scott, B. Dkhil, *Adv. Mater.* 26 (35) (2014) 6132–6137.
- [20] T. Tong, J. Karthik, R.V.K. Mangalam, L.W. Martin, D.G. Cahill, *Phys. Rev. B* 90 (9) (2014) 094116.
- [21] X.-D. Jian, B. Lu, D.-D. Li, Y.-B. Yao, T. Tao, B. Liang, J.-H. Guo, Y.-J. Zeng, J.-L. Chen, S.-G. Lu, *ACS Appl. Mater. Interfaces* 10 (5) (2018) 4801–4807.
- [22] X.-D. Jian, B. Lu, D.-D. Li, Y.-B. Yao, T. Tao, B. Liang, X.-W. Lin, J.-H. Guo, Y.-J. Zeng, S.-G. Lu, *ACS Appl. Mater. Interfaces* 11 (22) (2019) 20167–20173.
- [23] S.G. Lu, B. Rožič, Q.M. Zhang, Z. Kutnjak, R. Pirc, *Appl. Phys. A* 107 (3) (2012) 559–566.
- [24] S. Pandya, G.A. Velarde, R. Gao, A.S. Everhardt, J.D. Wilbur, R. Xu, J.T. Maher, J.C. Agar, C. Dames, L.W. Martin, *Adv. Mater.* 31 (5) (2019) 1803312.
- [25] G. Velarde, S. Pandya, L. Zhang, D. Garcia, E. Lupi, R. Gao, J.D. Wilbur, C. Dames, L.W. Martin, *ACS Appl. Mater. Interfaces* 11 (38) (2019) 35146–35154.
- [26] A.K. Kalyani, K. Brajesh, A. Senyshyn, R. Ranjan, *Appl. Phys. Lett.* 104 (25) (2014) 252906.
- [27] L. Zhang, X. Ren, M.A. Carpenter, *Phys. Rev. B* 95 (5) (2017) 054116.
- [28] W. Liu, X. Ren, *Phys. Rev. Lett.* 103 (25) (2009) 257602.
- [29] L. Zhang, M. Zhang, L. Wang, C. Zhou, Z. Zhang, Y. Yao, L. Zhang, D. Xue, X. Lou, X. Ren, *Appl. Phys. Lett.* 105 (16) (2014) 162908.
- [30] C. Zhou, W. Liu, D. Xue, X. Ren, H. Bao, J. Gao, L. Zhang, *Appl. Phys. Lett.* 100 (22) (2012) 222910.
- [31] M. Acosta, N. Khakpash, T. Someya, N. Novak, W. Jo, H. Nagata, G.A. Rossetti, J. Rödel, *Phys. Rev. B* 91 (10) (2015) 104108.
- [32] M.M. Vopson, *J. Phys. D Appl. Phys.* 46 (34) (2013) 345304.
- [33] A. Planes, T. Castán, A. Saxena, *Philos. Mag.* 94 (17) (2014) 1893–1908.
- [34] X. Zhang, L. Wu, S. Gao, J.Q. Liu, B. Xu, Y.D. Xia, J. Yin, Z.G. Liu, *AIP Adv.* 5 (4) (2015) 047134.
- [35] B.L. Cheng, M. Gabbay, W. Duffy, G. Fantozzi, *J. Mater. Sci.* 31 (18) (1996) 4951–4955.